Optics Communications 318 (2014) 47–52

Contents lists available at ScienceDirect

Optics Communications

journal homepage: www.elsevier.com/locate/optcom

SFM-FDTD analysis of triangular-lattice AAA structure: Parametric study of the TEM mode

M. Hamidi [a], C. Chemrouk [a], A. Belkhir [a,*], Z. Kebci [a], A. Ndao [b], O. Lamrous [a], F.I. Baida [b]

[a] Laboratoire de Physique et Chimie Quantique, Faculté des Sciences, Université Mouloud Mammeri Tizi-Ouzou BP 17 RP, 15000 Tizi-Ouzou, Algeria
[b] Département d'Optique P. M. Duffieux, Institut FEMTO-ST UMR 6174 CNRS, Université de Franche-Comté, 25030 Besançon Cedex, France

ARTICLE INFO

Article history:
Received 18 June 2013
Received in revised form
12 December 2013
Accepted 17 December 2013
Available online 3 January 2014

Keywords:
AAA structure
Triangular lattice
Photonic crystal
TEM mode
SFM-FDTD

ABSTRACT

This theoretical work reports a parametric study of enhanced transmission through annular aperture array (AAA) structure arranged in a triangular lattice. The effect of the incidence angle in addition to the inner and outer radii values on the evolution of the transmission spectra is carried out. To this end, a 3D Finite-Difference Time-Domain code based on the Split Field Method (SFM) is used to calculate the spectral response of the structure for any angle of incidence. In order to work through an orthogonal unit cell which presents the advantage to reduce time and space of computation, special periodic boundary conditions are implemented. This study provides a new modeling of AAA structures useful for producing tunable ultra-compact devices.

1. Introduction

Annular aperture arrays (AAA) are photonic crystals (PCs) that have known an increasing interest owing of their extraordinary optical transmission which can be exploited in a variety of ultra-compact optical devices. Very high transmission (up to 90%) through metallic coaxial apertures has been achieved via the excitation of the fundamental transverse electric mode (TE_{11}) inside the apertures [1]. In addition, it has been theoretically demonstrated that this kind of cavity allows the excitation of the cutoff-free *TEM* (transverse electromagnetic) guided mode. The generation of this mode is obtained by illuminating the structure under oblique incidence and by considering a TM polarization [2]. In this field of nano-optics, most of works deal with these PCs in rectangular lattices in order to enhance the transmission of the *TEM* mode [3–5]. This peculiar structure presents, as other PCs, a frequency bandgap in which the electromagnetic wave propagation is forbidden. This interesting property offers the possibility to control the light propagation and allows as well to consider many applications [6–8]. Let us mention that the bandgap width of these nanostructures strongly depends on the polarization and especially on the symmetry of the crystal. In contrast to the rectangular lattice, the triangular lattice is of great interest since it presents for some geometrical parameters, a total bandgap for both TE and TM polarizations [9]. In this context, it seems interesting to study the position of the *TEM* transmission peak through aperture arrays arranged in a triangular lattice according to their geometrical parameters and to the illumination direction.

Among the widely used methods, the Finite-Difference Time-Domain (FDTD) seems more appropriate to calculate the transmission spectra of these triangular-lattice PCs. However, in its classical formulation, the FDTD method is hampered by the implementation of boundary conditions. To overcome this problem, various methods have been proposed especially for the bandgap calculation. These include the non-orthogonal and the orthogonal methods using a rhombic unit cell [10,11] and a rectangular super cell [12] respectively. These methods have the drawback of being CPU-time and memory consumers. In addition, the first one (non-orthogonal) is not easy to implement and suffers from the late-time instability [13].

We report in this paper an adaptation of the SFM-FDTD method, previously developed for the rectangular lattice [14–16], in the general case of a 2D-periodic PC (finite in the third direction) arranged in a triangular lattice and illuminated at oblique incidence. Since the unit cell of triangular lattice is not rectangular, it is difficult to apply Yee's algorithm in its classical orthogonal formulation. So the implementation is achieved by choosing a rectangular unit cell and correctly adapting the periodic boundary conditions in order to avoid a folded version of the band diagram. This new approach has already been applied only for the 2D photonic bandgap calculations [9,17] and presents the advantage of being easy to implement with a considerable gain

* Corresponding author.
E-mail address: belkhir_abderahmane@ummto.dz (A. Belkhir).

0030-4018/$ - see front matter © 2013 Elsevier B.V. All rights reserved.
http://dx.doi.org/10.1016/j.optcom.2013.12.051

in computational time and space. In complementary to those studies [9,17], our aim is to extend this approach for general 3D calculations of transmission (and/or reflection) spectra at oblique incidence. After validation of our code, we have carried out an original parametric study dealing with annular aperture arrays (AAA) engraved into metallic layer.

So, this paper is organized as follows: the second section recalls the developments of the computational SFM-FDTD method employed in this study, including the modification and implementation of the special periodic conditions in case of triangular lattice. The third section gives performance tests of the resulting program and discusses about the enhanced optical transmission obtained through AAA arranged in a triangular lattice. More precisely, the influence of inner and outer radii on the resonance position and efficiency of the transmitted signal is studied. Finally, section four concludes this work and gives perspectives inspired from our results.

2. Theoretical development

SFM-FDTD code working in oblique incidence has already been implemented for the modeling of photonic crystals that are biperiodic structures (in x and y direction) and finished according to z direction. The algorithm takes into account the dispersion of noble metals described by the Drude, Drude–Lorentz [14,18] and Critical points model [16] according to the optical range and the nature of the considered noble metal. The originality of this code lies in the fact of being able to work in oblique incidence while keeping the frequency wide-band character of the method. Among the photonic crystals, the most studies include the rectangular and triangular lattices (Fig. 1) on which we will focus in this paper.

For a plane wave propagation along the $\vec{k}$ vector defined in the (xyz) coordinates system by incident and azimuthal angles θ and ϕ respectively (Fig. 2), the electric and magnetic fields can be expressed as

$$\vec{E} = \vec{E}_0\, e^{i(k_x\cdot x + k_y\cdot y + k_z\cdot z)} \tag{1}$$

$$\vec{H} = \vec{H}_0\, e^{i(k_x\cdot x + k_y\cdot y + k_z\cdot z)} \tag{2}$$

where $k_x = \omega/v\cdot \sin\theta\cdot\cos\phi$, $k_y = \omega/v\cdot \sin\theta\cdot\sin\phi$, $k_z = \omega/v\cdot\cos\theta$ and v is the light speed in the incident medium.

In the case of a 2D-periodic rectangular lattice (Fig. 1a), the boundary conditions, according to x and y directions, are given by the Floquet–Bloch periodic conditions as follows:

$$\vec{E}(x=a,y,t) = \vec{E}(x=0,y,t)e^{ik_x\cdot a} \tag{3}$$

$$\vec{E}(x,y=b,t) = \vec{E}(x,y=0,t)e^{ik_y\cdot b} \tag{4}$$

$$\vec{H}(x=0,y,t) = \vec{H}(x=a,y,t)e^{-ik_x\cdot a} \tag{5}$$

$$\vec{H}(x,y=0,t) = \vec{H}(x,y=b,t)e^{-ik_y\cdot b} \tag{6}$$

where a and b are the lattice constants.

Because of the emergence of the frequency term, the implementation of such conditions is not compatible with the purely temporal character of the traditional FDTD method. To rectify this situation, we have resorted to a change of variables in passing from $\vec{E}$ and $\vec{H}$ fields toward the new variables $\vec{P}$ and $\vec{Q}$ expressed as

$$\vec{P} = \vec{E}\, e^{-i(k_x x + k_y y)} \tag{7}$$

$$\vec{Q} = \vec{H}\, e^{-i(k_x x + k_y y)} \tag{8}$$

These new variables shall verify the periodic boundary conditions in a way similar to components of $\vec{E}$ and $\vec{H}$ for a normal incidence:

$$\vec{P}(x=a,y,z,t) = \vec{P}(x=0,y,z,t) \tag{9}$$

$$\vec{P}(x,y=b,z,t) = \vec{P}(x,y=0,z,t) \tag{10}$$

$$\vec{Q}(x=0,y,z,t) = \vec{Q}(x=a,y,z,t) \tag{11}$$

$$\vec{Q}(x,y=0,z,t) = \vec{Q}(x,y=b,z,t) \tag{12}$$

The direct implementation of these new variables in the Maxwell equations is not adapted to the classical Yee scheme. Therefore, new intermediate variables $\vec{P}_a$ and $\vec{Q}_a$ are then introduced by applying the Split Field Method (SFM) [19] and related to the global variables $\vec{P}$ and $\vec{Q}$. The open medium in the

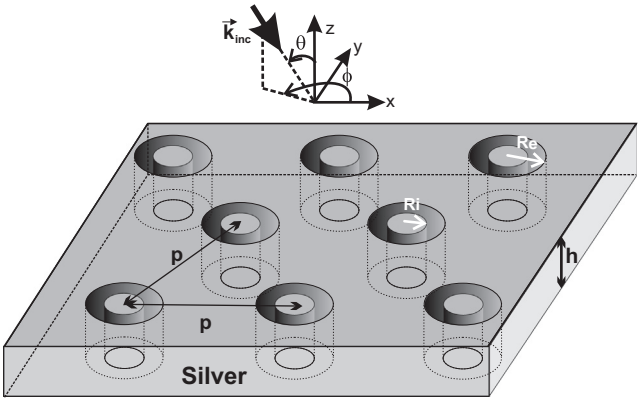

Fig. 2. Schematic of AAA structure arranged in a triangular lattice. R_i is the inner radius, R_e is the outer one, p is the grating period, θ is the angle of incidence and ϕ is the azimuthal angle.

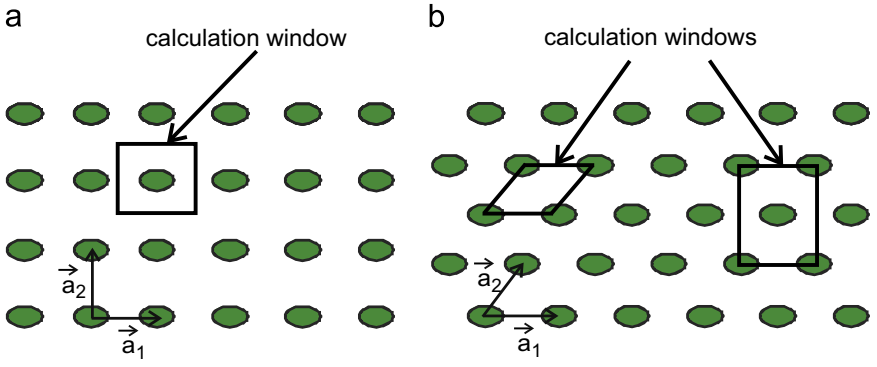

Fig. 1. (a) 2D rectangular lattice with unit vectors $\vec{a}_1 = a\,\vec{i}$ and $\vec{a}_2 = b\,\vec{j}$. (b) 2D triangular lattice with unit vectors $\vec{a}_1 = a\,\vec{i}$ and $\vec{a}_2 = (a/2)\,\vec{i} + (a\sqrt{3}/2)\,\vec{j}$. The most used FDTD calculation windows are also represented.

third direction is described by absorbing boundary conditions that are Berenger Perfectly Matched Layers (PML) [20,21]. The equations in the PML media are also adapted for the oblique case. They are expressed in the $\vec{P}-\vec{Q}$ domain and implemented using the SFM method. Relations and details are given in [14].

For the triangular lattice, the choice of the calculation window can be done in different ways. The first is to take a non-orthogonal unit cell (Fig. 1b) and implement the periodic boundary conditions in a Non-orthogonal-FDTD algorithm [10,11] where orthogonal FDTD is not suitable. With remaining in the orthogonal FDTD, a second choice would be to take a rectangular calculation window containing two patterns and lattice constants a and $a\sqrt{3}$ in Ox and Oy directions respectively (Fig. 1b). The Floquet-Bloch periodic conditions are applied in a similar manner to the case of the rectangular calculation window with a single pattern previously detailed.

In this paper, we have chosen to halve this rectangular window in a rectangular unit cell in order to use minimum computational time and space while remaining with the orthogonal FDTD algorithm (Fig. 3a). However, periodic boundary conditions must be adapted in order to describe exactly a periodic triangular lattice. This is done as follows (Fig. 3b):

- along the x direction:

$$\vec{E}(x=a,y,z,t)=\vec{E}(x=0,y,z,t)e^{ik_x\cdot a} \tag{13}$$

$$\vec{H}(x=0,y,z,t)=\vec{H}(x=a,y,z,t)e^{-ik_x\cdot a} \tag{14}$$

- along the y direction for $0\le x\le a/2$:

$$\vec{E}\left(x,y=\frac{a\sqrt{3}}{2},z,t\right)=\vec{E}\left(x+\frac{a}{2},y=0,z,t\right)e^{i(k_y\cdot a\sqrt{3}/2-k_x\cdot a/2)} \tag{15}$$

$$\vec{H}\left(x+\frac{a}{2},y=0,z,t\right)=\vec{H}\left(x,y=\frac{a\sqrt{3}}{2},z,t\right)e^{-i(k_y\cdot a\sqrt{3}/2-k_x\cdot a/2)} \tag{16}$$

- along the y direction for $a/2\le x\le a$:

$$\vec{E}\left(x,y=\frac{a\sqrt{3}}{2},z,t\right)=\vec{E}\left(x-\frac{a}{2},y=0,z,t\right)e^{i(k_y\cdot a\sqrt{3}/2+k_x\cdot a/2)} \tag{17}$$

$$\vec{H}\left(x-\frac{a}{2},y=0,z,t\right)=\vec{H}\left(x,y=\frac{a\sqrt{3}}{2},z,t\right)e^{-i(k_y\cdot a\sqrt{3}/2+k_x\cdot a/2)} \tag{18}$$

The above conditions are applied as they are in the case of dispersion diagram calculations [9,17] (k_x and k_y fixed) and in the 3D case of normal incidence ($k_x=k_y=0$) for the calculations of transmission and reflection spectra. In the general case, for 3D structures illuminated at oblique incidence, we have made the same change of variables as for rectangular lattice by introducing the $\vec{P}$ and $\vec{Q}$ variables. Thus, these new variables satisfy the following periodic boundary conditions:

- along the x direction:

$$\vec{P}(x=a,y,z,t)=\vec{P}(x=0,y,z,t) \tag{19}$$

$$\vec{Q}(x=0,y,z,t)=\vec{Q}(x=a,y,z,t) \tag{20}$$

- along the y direction for $0\le x\le a/2$:

$$\vec{P}\left(x,y=\frac{a\sqrt{3}}{2},z,t\right)=\vec{P}\left(x+\frac{a}{2},y=0,z,t\right) \tag{21}$$

$$\vec{Q}\left(x+\frac{a}{2},y=0,z,t\right)=\vec{Q}\left(x,y=\frac{a\sqrt{3}}{2},z,t\right) \tag{22}$$

- along the y direction for $a/2\le x\le a$:

$$\vec{P}\left(x,y=\frac{a\sqrt{3}}{2},z,t\right)=\vec{P}\left(x-\frac{a}{2},y=0,z,t\right) \tag{23}$$

$$\vec{Q}\left(x-\frac{a}{2},y=0,z,t\right)=\vec{Q}\left(x,y=\frac{a\sqrt{3}}{2},z,t\right) \tag{24}$$

Let us note that these new periodic conditions are also applied in the PML region.

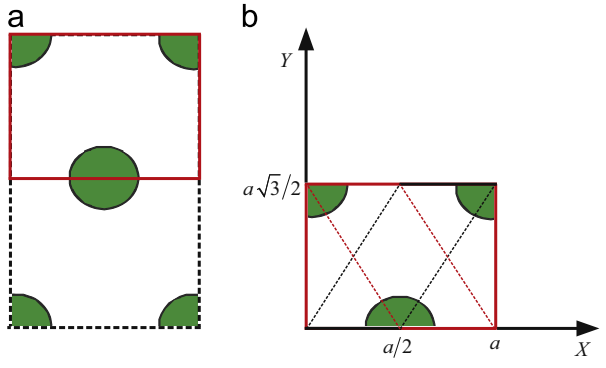

Fig. 3. (a) Rectangular window calculation in the classical FDTD algorithm containing two patterns reduced to (b) small rectangular unit cell with adapted boundary conditions.

3. Validation and simulation results

In this section, numerical results are presented in order to, first, validate our modified SFM-FDTD code and, second, to study the AAA structure. This last part deals with the properties of the *TEM* mode function of the AAA radii and the angle incidence values. The considered structure is made of silver film perforated with nanocoaxial apertures arranged in a triangular lattice (Fig. 2). The dispersion of the silver is described by the Drude model $\varepsilon(\omega)=1-\omega_p^2/(\omega^2+i\omega\gamma)$ with $\omega_p=1.38\times10^{16}$ rad/s and $\gamma=3.07\times10^{13}$ rad/s determined by fitting the experimental data of [22] in the visible domain.

The validation test is carried out by comparing the transmission spectra of the same AAA structure when considering two different calculation windows for both *TE* and *TM* polarizations at oblique incidence. The first calculation is done with the classical SFM-FDTD code, devoted to the rectangular lattice and successfully confronted with other methods in previous papers [14,15,18], in the case of a rectangular calculation window containing two patterns. The second one uses the modified SFM-FDTD code that takes into account the new periodic boundary conditions for a calculation window with only one pattern. As shown in Fig. 4, the two calculations (Fig. 4a for *TE* polarization and Fig. 4b for *TM* polarization) lead exactly to the same transmission spectra but with a 50% reduced memory space and then with a time gain of more than 60%. As previously demonstrated, an enhanced optical transmission (double peak between $\lambda=500$ nm and $\lambda=700$ nm) is obtained by the excitation of the TE_{11} guided mode [1,3,4,23] which almost corresponds to the spectral position of the transmission peak. In addition, in the case of oblique incidence with *TM* polarization (Fig. 4b), the *TEM* mode, which has no cutoff

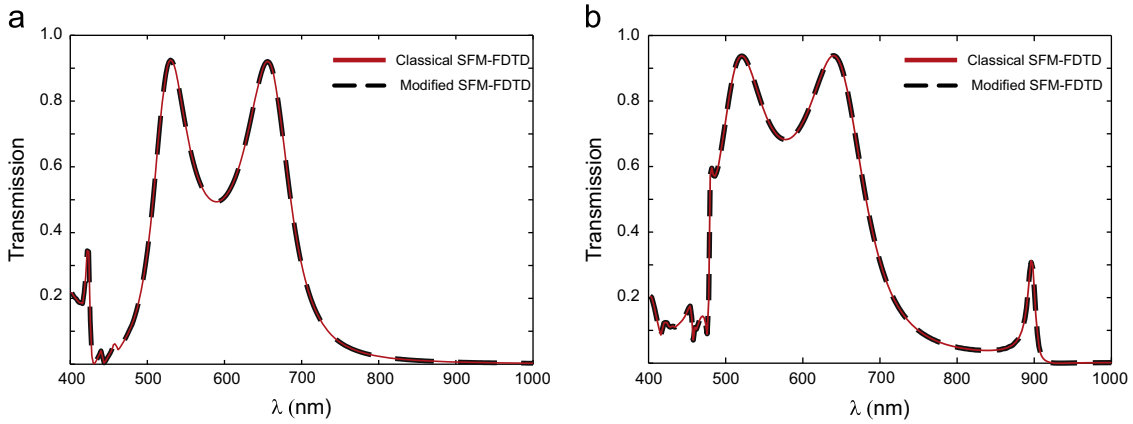

Fig. 4. Zero-order transmission coefficients versus the wavelength for the triangular AAA structure with $R_i = 50$ nm, $R_e = 100$ nm, $p = 300$ nm and $h = 240$ nm under oblique incidence ($\theta = 35°$). Comparison between the classical SFM-FDTD code and the modified one in case of (a) *TE* and (b) *TM* polarizations.

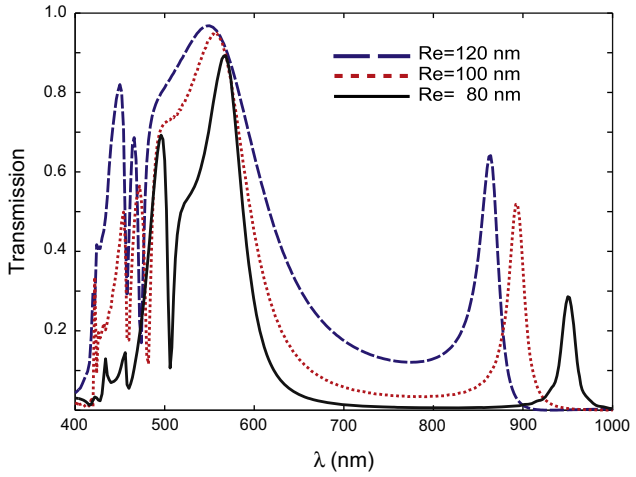

Fig. 5. Zero-order transmission spectra through the triangular AAA structure with $p = 300$ nm and $h = 240$ nm in case of oblique incidence. The outer radius is varied with $R_i = 40$ nm and $\theta = 55°$.

wavelength, is excited and allows enhanced transmission at wavelength larger than the TE_{11} mode one.

The flexibility of this optimized code naturally allows us to achieve a parametric study on the position and the amplitude of the *TEM*-based transmission peak. Indeed, in addition to the dispersion of the metal, the position of this peak as well as its intensity strongly depend on the geometrical parameters. The *TEM* mode wavelength is given by the following relationship [5]:

$$\lambda_{TEM} = \frac{2\pi n_{eff}\, h}{l\pi - \phi_r} \tag{25}$$

where n_{eff} is the real part of the effective index of the *TEM* mode, ϕ_r is the phase change induced by the reflection on the two ends of the coaxial waveguide, h is the metal film thickness and l is a non-zero positive integer. If it is obvious that an increase in the metal thickness induces a redshift for the *TEM* peak, the influence of inner and outer radii is not explicitly studied. In fact, the phase ϕ_r depends on the radii of the apertures because it involves evanescent waves that are diffracted by the end of the structure. In addition, and contrarily to the case of a perfect conductor, the effective index n_{eff} of the *TEM* plasmonic guided mode (case of real dispersive metals) depends on the radii values and on the metal dispersion. Fig. 5 illustrates these properties and shows that the *TEM* peak spectral position varies according to the outer radius for fixed values of the inner one and of the metal thickness. The observed redshift can be then understood, through the relation (25), by an increasing of the phase change ϕ_r and/or the effective index n_{eff}. Let us note that the *TEM* redshift is accompanied by a decrease in the transmission efficiency. This latter is attributed to the spatial extension properties of the *TEM* mode that penetrates more importantly into the metal part of the structure. In order to enhance the *TEM*-based transmission, we consider in the following the tilted AAA structure illuminating at normal incidence. This configuration was recently proposed and studied in the range of GHz frequency [24]. In fact, the obtained results in [5] showed an improved transmission compared to the conventional structure illuminated at oblique incidence.

The effect of the inner radius is studied within this new structure as shown in Fig. 6a. The behavior of the *TEM* position is identical to that observed previously (redshift when decreasing the inter conductors distance) but with a better transmission efficiency. In order to decouple the effects of the real part of the effective index from the one of the phase change, mentioned above, we calculate the dispersion curve of the *TEM* mode for different values of R_i (see Fig. 6b) at a fixed value of $R_e = 130$ nm. For each couple (R_e, R_i), an almost linear evolution of the frequency ω versus k_z is obtained leading to a quite constant value of the effective index real part which is given by the relation $k_z c/\omega$. Nevertheless, the value of n_{eff} increases with the inner radius ($n_{eff} = 1.39, 1.51$ and 1.88 for $R_i = 70$ nm, 90 nm and 110 nm respectively). Furthermore, the values of the phase change ϕ_r can be deduced from Fig. 6a (λ_{TEM}) and Fig. 6b (n_{eff}) by using Eq. (25). This leads to the values $\phi_r = 53.96°$, $61.42°$ and $69.58°$ respectively.

A complete quantitative study on the influence of the radii values is presented in Fig. 7 by calculating the transmission spectra of a tilted AAA structure and extracting, for each couple (R_i, R_e), the position (Fig. 7a) and the transmission efficiency (Fig. 7b) of the *TEM*-based peak. More the inner conductors distance is low (i.e. R_e (R_i) approaches R_i (R_e)), more the TEM pick is shifted to the larger wavelengths. Similarly, the transmission coefficient decreases when the fill rate of annular holes decreases (i.e. R_e and R_i lowers).

As can be seen in Fig. 7a, the redshift does not follow the same trend when the decrease of the inter conductors distance is obtained by fixing R_i and reducing R_e or by fixing R_e and increasing R_i. Indeed, this redshift is more pronounced for the last case and this behavior can also be explained by the competition of the effects induced by n_{eff} and ϕ_r according to Eq. (25). To illustrate this purpose, we plot in Fig. 8, the variation of these two quantities versus $R_i(R_e)$ with R_e (R_i) fixed. According to Fig. 8a, we confirm that when R_i increases, ϕ_r and n_{eff} increase together. Both effects add up and contribute to the redshift. In contrast, when R_e decreases for R_i fixed (see Fig. 8b), the two effects are opposite. In this last case (for the AAA structure made in silver), the effect of

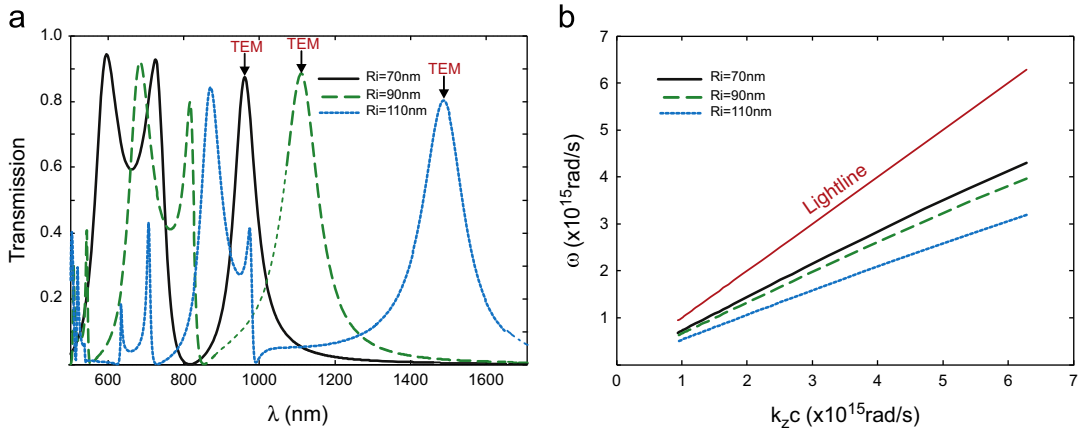

Fig. 6. (a) Zero-order transmission spectra through tilted triangular AAA structure of 25° with $p = 400$ nm and $h = 220$ nm in case of normal incidence. (b) Dispersion curves for the same structure. The inner radius is varied with $R_e = 130$ nm.

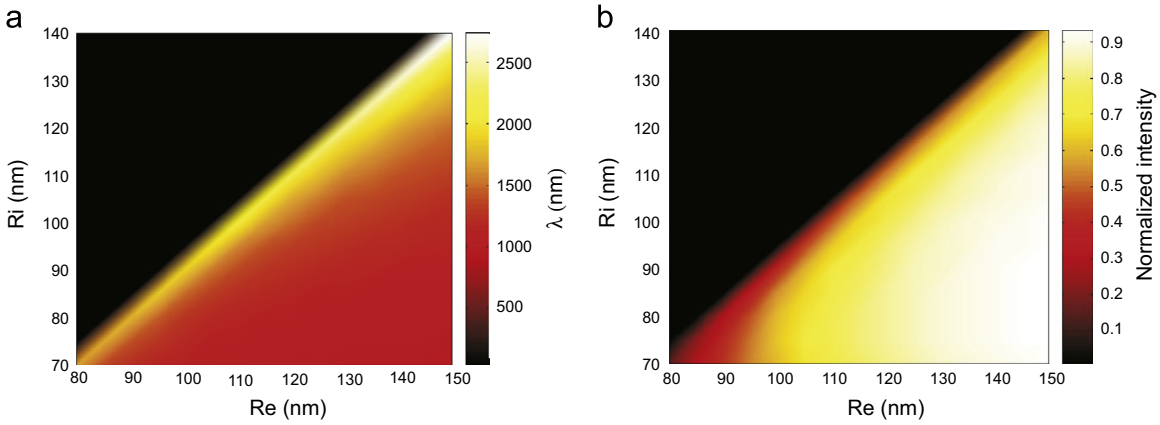

Fig. 7. (a) TEM mode wavelengths and (b) intensity for different values of R_e and R_i of the 25° tilted triangular AAA structure ($p = 400$ nm and $h = 220$ nm) in case of normal incidence.

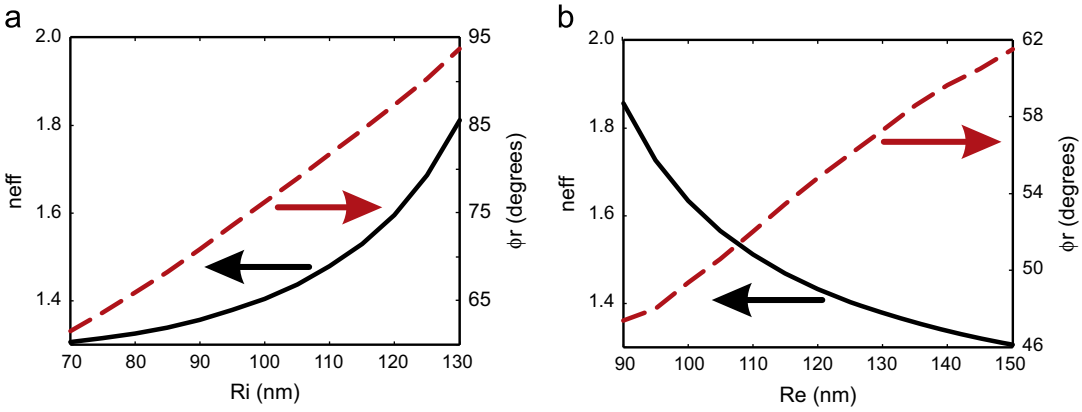

Fig. 8. Evolution of the real part of the effective index and the phase change within the 25° tilted triangular AAA structure ($p = 400$ nm and $h = 220$ nm) in case of normal incidence. (a) The inner radius is varied with $R_e = 150$ nm. (b) The outer radius is varied with $R_i = 70$ nm.

n_{eff} outweighs ϕ_r and explains the weak evolution of the peak position. Thus, for microwave's applications, when the metal can be considered perfect (n_{eff} remains equal to 1), the TEM mode would be only shifted to the blue region of the spectrum when reducing R_e for fixed R_i.

4. Conclusion

In this paper we have developed an SFM-FDTD code, working in oblique incidence, with adapted periodic boundary conditions for calculation of transmission and reflection spectra in case of triangular lattices that are finite according to the third direction. To model the free space in this last direction, PML of Berenger are adapted. The choice of a reduced rectangular unit cell enables us to work in orthogonal FDTD and leads us to minimize the computational space and time. Validation tests are presented in order to demonstrate the accuracy of this algorithm. This code is then applied to the parametric study of the *TEM* mode for AAA structure made in silver. The effect of the outer and inner radii is studied in order to follow the evolution of the associated wavelength and transmission efficiency. It shows a strong dependence of the peak

position with the distance separating the two metallic interfaces of the coaxial waveguide. This dependence of the *TEM* peak position versus the radii could be exploited to tune the enhanced transmission in this kind of structures.

Acknowledgments

This work is partly supported by the Algerian "Projet National de Recherche no. 8/u15/1096/2011" and by the Labex ACTION (CNRS France).

References

[1] Y. Poujet, J. Salvi, F.I. Baida, Opt. Lett. 32 (20) (2007) 2942, URL: ⟨http://ol.osa.org/abstract.cfm?URI=ol-32-20-2942⟩.
[2] F.I. Baida, Appl. Phys. B: Lasers Opt. 89 (2007) 145, http://dx.doi.org/10.1007/s00340-007-2787-3.
[3] S.M. Orbons, M.I. Haftel, C. Schlockermann, D. Freeman, M. Milicevic, T.J. Davis, B. Luther-Davies, D.N. Jamieson, A. Roberts, Opt. Lett. 33 (8) (2008) 821, URL: ⟨http://ol.osa.org/abstract.cfm?URI=ol-33-8-821⟩.
[4] F.I. Baida, Y. Poujet, J. Salvi, D.V. Labeke, B. Guizal, Opt. Commun. 282 (7) (2009) 1463, URL: ⟨http://www.sciencedirect.com/science/article/pii/S0030401808012637⟩.
[5] F.I. Baida, A. Belkhir, O. Arar, E. Barakat, J. Dahdah, C. Chemrouk, D.V. Labeke, C. Diebold, N. Perry, M.-P. Bernal, Micron 41 (7) (2010) 742, URL: ⟨http://www.sciencedirect.com/science/article/pii/S0968432810001460⟩.
[6] T.W. Ebbesen, H.J. Lezec, H.F. Ghaemi, T. Thio, P.A. Wolff, Nature 391 (6668) (1998) 667, http://dx.doi.org/10.1038/35570.
[7] F.I. Baida, D.V. Labeke, Opt. Commun. 209 (2002) 17, URL: ⟨http://www.sciencedirect.com/science/article/pii/S0030401802016905⟩.
[8] D.V. Labeke, D. Gérard, B. Guizal, F.I. Baida, L. Li, Opt. Express 14 (25) (2006) 11945, URL: ⟨http://www.opticsexpress.org/abstract.cfm?URI=oe-14-25-11945⟩.
[9] A. Belkhir, Extension de la modélisation par FDTD en nano-optique (Thesis), Université de Franche-Comte, Besançon, 2008. URL: ⟨http://tel.archives-ouvertes.fr/tel-00373606/en/⟩.
[10] M. Qiu, Computational methods for the analysis and design of photonic bandgap structures (Ph.D.), Royal Institute of Technology, Stockholm, 2000. URL: ⟨http://urn.kb.se/resolve?urn=urn:nbn:se:kth:diva-3037⟩.
[11] W. Kuang, W.J. Kim, J.D. O'Brien, J. Lightwave Technol. 25 (9) (2007) 2612, URL: ⟨http://jlt.osa.org/abstract.cfm?URI=jlt-25-9-2612⟩.
[12] A. Chutinan, S. Noda, Phys. Rev. B 62 (2000) 4488, URL: ⟨http://link.aps.org/doi/10.1103/PhysRevB.62.4488⟩.
[13] J. Liu, M. Brio, J. Moloney, J. Sci. Comput. 39 (2009) 129, http://dx.doi.org/10.1007/s10915-008-9253-1.
[14] A. Belkhir, F.I. Baida, Phys. Rev. E 77 (5) (2008) 056701, URL: ⟨http://link.aps.org/doi/10.1103/PhysRevE.77.056701⟩.
[15] F.I. Baida, A. Belkhir, Opt. Lett. 34 (16) (2009) 2453, URL: ⟨http://ol.osa.org/abstract.cfm?URI=ol-34-16-2453⟩.
[16] M. Hamidi, F.I. Baida, A. Belkhir, O. Lamrous, J. Phys. D: Appl. Phys. 44 (24) (2011) 245101, URL: ⟨http://stacks.iop.org/0022-3727/44/i=24/a=245101⟩.
[17] A.V. Umenyi, K. Miura, O. Hanaizumi, J. Lightwave Technol. 27 (22) (2009) 4995, URL: ⟨http://ieeexplore.ieee.org/xpl/articleDetails.jsp?arnumber=5165014⟩.
[18] A. Belkhir, O. Arar, S.S. Benabbes, O. Lamrous, F.I. Baida, Phys. Rev. E 81 (4) (2010) 046705, URL: ⟨http://link.aps.org/doi/10.1103/PhysRevE.81.046705⟩.
[19] M. Veysoglu, R. Shin, J. Kong, J. Electromagn. Waves Appl. 7 (12) (1993) 1595, URL: ⟨http://w ww.tandfonline.com/doi/abs/10.1163/156939393X00020⟩.
[20] J.-P. Berenger, J. Comput. Phys. 114 (2) (1994) 185, URL: ⟨http://www.sciencedirect.com/science/article/pii/S0021999184711594⟩.
[21] J.-P. Berenger, J. Comput. Phys. 127 (2) (1996) 363, URL: ⟨http://www.sciencedirect.com/science/article/pii/S0021999196901813⟩.
[22] P.B. Johnson, R.W. Christy, Phys. Rev. B 6 (1972) 4370, URL: ⟨http://link.aps.org/doi/10.1103/PhysRevB.6.4370⟩.
[23] F.I. Baida, Y. Poujet, B. Guizal, D.V. Labeke, Opt. Commun. 256 (2005) 190, URL: ⟨http://www.sciencedirect.com/science/article/pii/S0030401805006760⟩.
[24] S. Nosal, Modélisation electromagnétique de structures périodiques et matériqux artificiels. application à la conception d'un radôme passe-bande (Ph.D. thesis), Ecole Centrale Paris, 2009.